

Communication

# Two Novel Pyrene Tetra-Sulfonate Europium Coordination Polymers: Structure Formation Mechanism Analysis and Sequential Modulation Strategy

Haoran Li <sup>1</sup>, Xiaolian Sun <sup>2</sup>, Jiaju Fu <sup>3,\*</sup> and Wenlei Zhu <sup>3,\*</sup> 

<sup>1</sup> Public Foundational Courses Department, Nanjing Vocational University of Industry Technology, Nanjing 210023, China

<sup>2</sup> State Key Laboratory of Natural Medicines, Key Laboratory of Drug Quality Control and Pharmacovigilance, Department of Pharmaceutics, China Pharmaceutical University, Nanjing 210009, China

<sup>3</sup> State Key Laboratory of Pollution Control and Resource Reuse, State Key Laboratory of Analytical Chemistry for Life Science, The Frontiers Science Center for Critical Earth Material Cycling, School of the Environment, School of Chemistry and Chemical Engineering, Nanjing University, Nanjing 210023, China

\* Correspondence: fujiaju123-123@163.com (J.F.); wenleizhu@nju.edu.cn (W.Z.)

**Abstract:** For the purpose of broadening the understanding of the sulfonic acid coordination mechanism, a coordination system consisting of Eu(III) ion and 1,3,6,8-pyrene tetra-sulfonate (1,3,6,8-PTS) ligand was chosen as the typical research object. By step regulating the volume ratio of mixed solvents and the molar ratio of metal salts to ligands, two pyrene tetra-sulfonate europium coordination polymers,  $\text{Eu}_6(\mu_6\text{-O})(\mu_3\text{-OH})_8(\text{NO}_3)_6(1,3,6,8\text{-H}_2\text{PTS})(\text{H}_2\text{O})_{10}$  (**1**) and  $\text{Eu}(\text{NO}_3)(1,3,6,8\text{-PTS})_{0.5}(\text{H}_2\text{O})_3 \cdot 0.5\text{bipy}$  (**2**), were obtained in sequence. Compound **1** shows a 1D chain-like structure interconnected with 1,3,6,8-PTS bridging ligands and rare  $[\text{Eu}_6(\mu_6\text{-O})(\mu_3\text{-OH})_8(\text{NO}_3)_6]^{2+}$  cluster nodes, while compound **2** shows a 2D layered structure. Further structural comparison with compound  $\text{Eu}(1,3,6,8\text{-PTS})(\text{H}_2\text{O})_7 \cdot 4\text{H}_2\text{O} \cdot \text{Hbipy}$  (**EuPTSbp-1**) was discussed in detail and the structure formation mechanism was analyzed. On this basis, a sequential modulation strategy for pyrene tetra-sulfonate europium coordination polymers was proposed.

**Keywords:** MOCPs; aryl sulfonic acid; coordination modes; crystal structure regulation



**Citation:** Li, H.; Sun, X.; Fu, J.;

Zhu, W. Two Novel Pyrene

Tetra-Sulfonate Europium

Coordination Polymers: Structure

Formation Mechanism Analysis and

Sequential Modulation Strategy.

*Crystals* **2022**, *12*, 1818. [https://](https://doi.org/10.3390/cryst12121818)

[doi.org/10.3390/cryst12121818](https://doi.org/10.3390/cryst12121818)

Academic Editor: Andrea Ienco

Received: 30 October 2022

Accepted: 8 December 2022

Published: 14 December 2022

**Publisher's Note:** MDPI stays neutral with regard to jurisdictional claims in published maps and institutional affiliations.



**Copyright:** © 2022 by the authors.

Licensee MDPI, Basel, Switzerland.

This article is an open access article

distributed under the terms and

conditions of the Creative Commons

Attribution (CC BY) license ([https://](https://creativecommons.org/licenses/by/4.0/)

[creativecommons.org/licenses/by/](https://creativecommons.org/licenses/by/4.0/)

[4.0/](https://creativecommons.org/licenses/by/4.0/)).

## 1. Introduction

Metal–organic coordination polymers (MOCPs), or commonly known as metal–organic frameworks (MOFs) or metal–organic coordination networks (MOCNs) in some cases, usually refer to coordination compounds with a periodic extended infinitely in a one-dimensional, two-dimensional, or three-dimensional network structure formed by the coordination of bonds between metal ions and organic ligands. They have diverse and easily modified skeletal structures, and many of them also have a functionalized pore structure with large porosity and specific surface area. These intriguing features lead widespread applications including gas storage and separation, catalysis, fluorescence sensing, optoelectronics, magnetic materials, bioengineering, and so on [1–15]. In recent years, MOCPs have also received extensive attention as precursors and templates for the preparation of various kinds of derivatives, including nanostructured carbon; metal oxides (MOs); metal composites (M/MO@C); and other metal-containing compounds such as metal nitrides (MNs), metal carbides (MCs), and so on [16–26]. As the properties of MOCPs and even their derivatives are significantly affected by the MOCPs' structures, it is crucial to have a fundamental understanding of the effects of synthesis conditions (e.g., temperature, solvent environment, pH, reagent concentration and molar ratio, the presence of counter ions, and template reagent, among others) for structure regulation [27–31].

As the essential components of MOCPs, the coordination habit of metal ion centers and various organic ligands can easily become research hotspots. Among them, aryl

sulfonic acid ligands have attracted extensive attention in recent years owing to their flexible coordination modes, including but not limited to  $\eta^1$ ,  $\eta^2$ ,  $\eta^2\mu_2$ ,  $\eta^1\mu_2$ ,  $\eta^3\mu_3$ , and so on [32–34]. Besides, sulfonic-acid-derived MOCPs exhibit excellent structural stability and excellent biocompatibility in general [35–39]. However, the studies on the regulation of sulfonic acid coordination mode are still lacking. Therefore, it's worth the effort to study the factors that affect coordination modes and explore a sequential modulation strategy for aryl sulfonic-acid-derived MOCPs.

In this work, Eu(III) ion and 1,3,6,8-pyrenetetra-sulfonic (1,3,6,8-PTS) ligand were selected as research objects for the following reasons: (1) rare earth ions are easily coordinated with oxygen and may be sensitive to aqueous mixed solvent systems; (2) the PTS ligand with a large conjugated system and four sulfonic groups can easily form various kinds of  $\pi$ – $\pi$  interactions and bridge connections, potentially increasing the coordination flexibility.

Previously, we reported an MOCP named  $\text{Eu}(1,3,6,8\text{-PTS})(\text{H}_2\text{O})_7 \cdot 4\text{H}_2\text{O} \cdot \text{Hbipy}$  (now abbreviated as **EuPTSbp-1**) [40]. The unique structure provides a 1D snake-shaped chain structure with the aid of the  $\pi$ – $\pi$  stacking effect of the 4,4'-bipyridine auxiliary template. For the purpose of exploring the sequential modulation strategy for pyrene tetrasulfonate europium coordination polymers (EuPTS-CPs), a series of solvothermal synthesis experiments were carried out and two EuPTS-CPs with different crystallographic structures were successively obtained. Their crystal structures were described and compared with **EuPTSbp-1** in detail.

## 2. Materials and Methods

All starting materials and solvents were obtained from commercial sources and used without further purification.

### 2.1. Synthesis of $\text{Eu}_6(\mu_6\text{-O})(\mu_3\text{-OH})_8(\text{NO}_3)_6(1,3,6,8\text{-H}_2\text{PTS})(\text{H}_2\text{O})_{10}$ (**1**)

In a typical synthesis procedure, a mixture of 1,3,6,8-pyrenetetra-sulfonic acid tetrasodium salt (1,3,6,8-PTS, 1.25 mmol, 0.763 g),  $\text{Eu}(\text{NO}_3)_3 \cdot 6\text{H}_2\text{O}$  (1.25 mmol, 0.558g), and 4,4'-bipyridine (1.25 mmol, 0.195 g) was added into a 25 mL Teflon inner liner, followed by the addition of 0.5 mL distilled water and 4.5 mL anhydrous ethanol. After stirring for 5 min, the Teflon inner liner was sealed into a stainless-steel vessel, heated to 90 °C within 120 min, kept at 90 °C for 3 days, and cooled to room temperature for 3 days. A mixture of the compound **1** and residue of yellow precipitation and structurally unknown yellow polycrystalline was obtained; no compound **2** or compound **EuPTSbp-1** was found in this mixture. Colorless prism shaped crystal samples for single crystal X-ray diffraction analysis were carefully picked manually from the mixture, under an optical microscope. For the purpose of obtaining the pure phase for compound **1**, many efforts were made to optimize the synthesis conditions, but they turned out to fail.

### 2.2. Synthesis of $\text{Eu}(\text{NO}_3)(1,3,6,8\text{-PTS})_{0.5}(\text{H}_2\text{O})_3 \cdot 0.5\text{bipy}$ (**2**)

In a typical synthesis procedure, a mixture of 1,3,6,8-pyrenetetra-sulfonic acid tetrasodium salt (1,3,6,8-PTS, 1.25 mmol, 0.763 g),  $\text{Eu}(\text{NO}_3)_3 \cdot 6\text{H}_2\text{O}$  (15 mmol, 6.692 g), and 4,4'-bipyridine (1.25 mmol, 0.195g) was added into a 25 mL Teflon inner liner, followed by the addition of 1.0 mL distilled water and 9.0 mL anhydrous ethanol. After stirring for 5 min, the Teflon inner liner was sealed into a stainless-steel vessel, heated to 90 °C within 120 min, kept at 90 °C for 3 days, and cooled to room temperature for 3 days. A mixture of compound **2** and the residue of yellow precipitation and structurally unknown colorless polycrystalline was obtained; no compound **1** or compound **EuPTSbp-1** was found in this mixture. Colorless flake crystal samples for single crystal X-ray diffraction analysis were carefully picked manually from the mixture, under an optical microscope. In order to obtain the pure phase for compound **2**, many experiments were carried out to optimize the synthesis conditions, but the results were unsuccessful.

### 2.3. X-ray Crystallographic Study

The single crystal X-ray diffraction intensity data of compounds **1** and **2** were collected on a Saturn 724HG CCD single crystal X-ray diffractometer using a graphite-monochromatic Mo K $\alpha$  radiation ( $\lambda = 0.71073 \text{ \AA}$ ) at 153K under N<sub>2</sub> flow. Diffraction intensity data were corrected by CrystalClear program (version 1.3.6). Using Olex2 (version 1.3.0) [41], the structure was solved with the olex2.solve [42] structure solution program using Charge Flipping and refined with the SHELXL (version 2018/3) [43] refinement package using least squares minimisation. A solvent mask supported by Olex2 was used to omit the free solvent molecules in compound **1**. The volume of these voids is 527.9  $\text{\AA}^3$  based on the formula unit. All nonhydrogen atoms were refined anisotropically. Hydrogen atoms were generated at geometrically calculated positions. The relevant crystallographic data and structure determination are listed in Table 1. The nearest metal–metal distance [ $\text{\AA}$ ] and main bond length [ $\text{\AA}$ ], and bond angle [ $^\circ$ ] in compound **1** and **2** are listed in Tables S1 and S2. CCDC 2213150 and 2213151 contain the supplementary crystallographic data. These data can be obtained free of charge via <https://www.ccdc.cam.ac.uk/structures/> (accessed on 11 December 2022) or from the CCDC, 12 Union Road, Cambridge CB2 1EZ, UK; Fax: +44-1223-336033; E-mail: deposit@ccdc.cam.ac.uk.

**Table 1.** Crystal data and structure refinement parameters for compounds **1**–**2**.

Compounds	1	2
Empirical formula	C <sub>16</sub> H <sub>36</sub> O <sub>49</sub> N <sub>6</sub> S <sub>4</sub> Eu <sub>6</sub> *	C <sub>13</sub> H <sub>13</sub> O <sub>12</sub> N <sub>2</sub> S <sub>2</sub> Eu
Formula weight	2136.51	605.33
Color and habit	Colorless Prism	Colorless Flake
Crystal system	Triclinic	Triclinic
Space group	<i>P</i> -1	<i>P</i> -1
<i>a</i> ( $\text{\AA}$ )	9.658(11)	7.376(5)
<i>b</i> ( $\text{\AA}$ )	10.668(14)	11.682(9)
<i>c</i> ( $\text{\AA}$ )	17.12(2)	11.757(9)
$\alpha$ ( $^\circ$ )	89.46(4)	110.813(10)
$\beta$ ( $^\circ$ )	82.75(5)	104.856(9)
$\gamma$ ( $^\circ$ )	81.24(3)	95.367(3)
<i>V</i> ( $\text{\AA}^3$ )	1729(4)	896.0(12)
<i>Z</i>	1	2
<i>D</i> <sub>c</sub> (g cm <sup>−3</sup> )	2.052	2.244
$\mu$ (mm <sup>−1</sup> )	5.578	3.806
<i>F</i> (000)	1008	592
$\theta$ range ( $^\circ$ )	3.02 to 27.42	2.96 to 27.53
<i>h, k, l</i> , ranges	−12 to 12, −13 to 13, −21 to 21	−9 to 9, −15 to 15, −15 to 15
<i>T</i> /K	153(2)	153(2)
<i>R</i> <sub>1</sub> , <sup>a</sup> <i>wR</i> <sub>2</sub> <sup>b</sup> [ <i>I</i> > 2 $\sigma$ ( <i>I</i> )]	0.0868, 0.2394	0.0479, 0.1118
<i>GOF</i> on <i>F</i> <sup>2</sup>	1.008	0.993

<sup>a</sup>  $R_1 = \sum ||F_o| - |F_c|| / \sum |F_o|$ . <sup>b</sup>  $wR_2 = [\sum w(F_o^2 - F_c^2)^2 / \sum w(F_o^2)^2]^{1/2}$ . \* The listed parameters do not take into account the full chemistry of compound **1**.

## 3. Results and Discussion

### 3.1. Crystal Structure

As mentioned above, compounds **1** and **2** with two different crystal structures were synthesized by the solvothermal method, with different metal/ligands molar ratio in reactants. It is a pity that the pure phase for neither compound **1** nor compound **2** was obtained in the end, despite a series of attempts. The crystal samples for single crystal X-ray diffraction analysis were picked manually from the corresponding impure products under an optical microscope. Nevertheless, crystal samples of compounds **1** and **2** are still reproducible, and discussing the crystal structure evolution of compounds **EuPTSbp-1** to **1**

to **2** with the change of solvothermal synthesis conditions is still of positive significance for studying the coordination habit of aryl sulfonic acids.

### 3.1.1. $\text{Eu}_6(\mu_6\text{-O})(\mu_3\text{-OH})_8(\text{NO}_3)_6(1,3,6,8\text{-H}_2\text{PTS})(\text{H}_2\text{O})_{10}$ (**1**)

According to single crystal X-ray diffraction data, compound **1** belongs to the triclinic  $P\bar{1}$  space group. As shown in Figure 1a,  $[\text{Eu}_6(\mu_6\text{-O})(\mu_3\text{-OH})_8(\text{NO}_3)_6]^{2+}$  hexanuclear europium oxygen cluster nodes were contained in compound **1**. In this europium oxygen cluster, six Eu(III) ions are connected by eight  $\mu_3\text{-OH}$  group and one  $\mu_6\text{-O}^{2-}$  ion to form an eight-caped octahedron structure, of which Eu(III) ions,  $\mu_3\text{-OH}$  groups, and  $\mu_6\text{-O}^{2-}$  ion are located at the vertices, the face-centers, and the body center, respectively, as shown in Figure 1b. Besides these bridge-linked oxygen atoms, Eu2 is coordinated by two oxygen atoms from coordinated  $\text{H}_2\text{O}$  molecules and chelated by two oxygen atoms from one  $\text{NO}_3^-$  ion. The coordination environment of Eu3 is similar to that of Eu2, but the spatial orientation of coordination groups is different. For Eu1, a coordinated oxygen atom from  $\text{H}_2\text{O}$  is replaced by an oxygen atom from the ligand sulfonic acid group, in which way two 1,3,6,8-PTS ligands are connected by the europium oxygen clusters to form 1D chains, as shown in Figure 2. Such 1D chains pack through weak interactions and form the spatial structure of compound **1**, as shown in Figure 3. For demonstrating the asymmetric unit in compound **1**, an ORTEP representation is shown in Figure S1. By simplifying the europium oxygen clusters to a node and the 1,3,6,8-pyrene tetra-sulfonic acid ligand to a two-connected node, the simple 1D chain-like structure topology diagram of compound **1** was obtained, as shown in Figure S2.

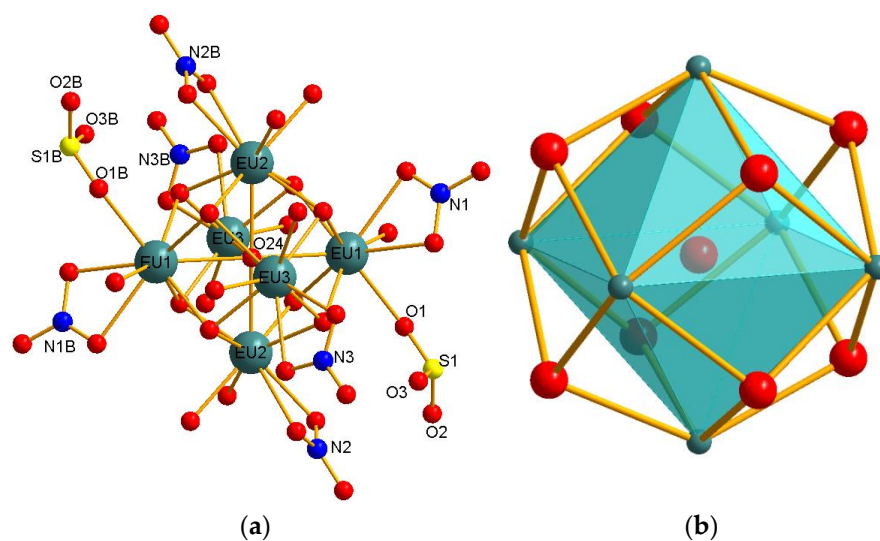


**Figure 1.** (a) Coordination environment of the Eu(III) ions in compound **1**; (b) hexanuclear Eu(III)-O clusters in compound **1**. Symmetry codes: (A)  $-x + 2, -y + 4, -z + 2$ ; (B)  $-x + 3, -y + 4, -z + 1$  (the C atoms and H atoms were omitted for clarity).

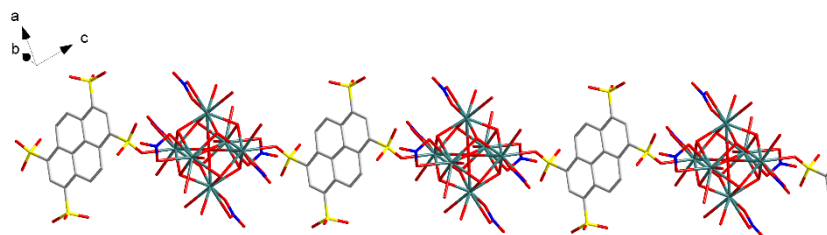


**Figure 2.** One-dimensional chain-like structure in compound **1**.

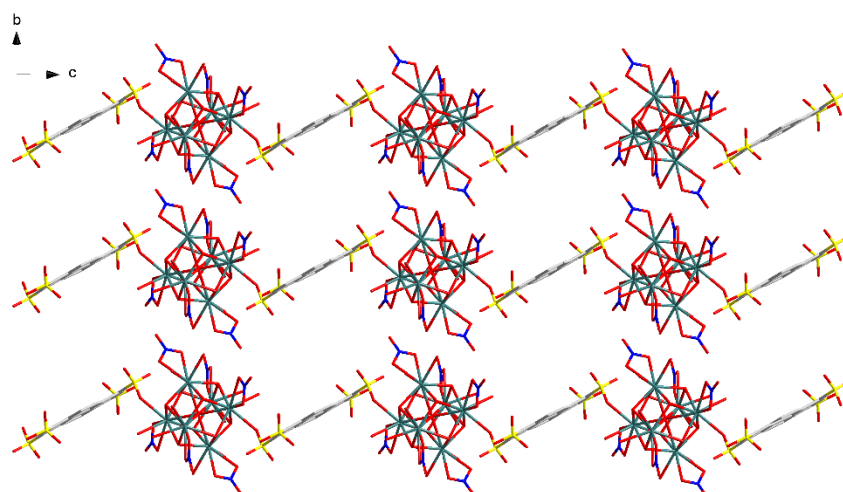


**Figure 3.** The packed chain-like structure in compound **1** along the *a* direction.

### 3.1.2. $\text{Eu}(\text{NO}_3)(1,3,6,8\text{-PTS})_{0.5}(\text{H}_2\text{O})_3 \cdot 0.5\text{bipy}$ (**2**)

According to the single crystal X-ray diffraction data, compound **2** belongs to the triclinic  $\overline{P1}$  space group. As shown in Figure 4, each Eu(III) ion is coordinated with three oxygen atoms (O1, O2, and O4) from two sulfonic acid groups of 1,3,6,8-pyrene tetra-sulfonic acid ligands and three oxygen atoms (O10, O11, and O12) from coordinated  $\text{H}_2\text{O}$  molecules, and is chelated by two oxygen atoms from one  $\text{NO}_3^-$  ion, showing an eight-coordinate configuration. For demonstrating the asymmetric unit in compound **2**, an ORTEP representation is shown in Figure S3. A 2D layered structure is formed by the 1,3,6,8-pyrene tetra-sulfonic acid ligands connecting the Eu(III) ion nodes, as shown in Figure 5. The sulfonic acid groups of pyrene tetra-sulfonic acid ligands are coordinated with Eu(III) ions in two different modes. One is to connect one Eu(III) ion node in a  $\eta^1$  way, and the other is to connect two Eu(III) ion nodes in the form of  $\eta^2-\mu_2$  mode. By simplifying the 1,3,6,8-pyrene tetra-sulfonic acid ligand to a four-connected node, the layered structure topology diagram of compound **2** can be obtained, as shown in Figure 5b. The Schläfli symbol can be expressed as  $(3^{33} \cdot 4^{33})$ .

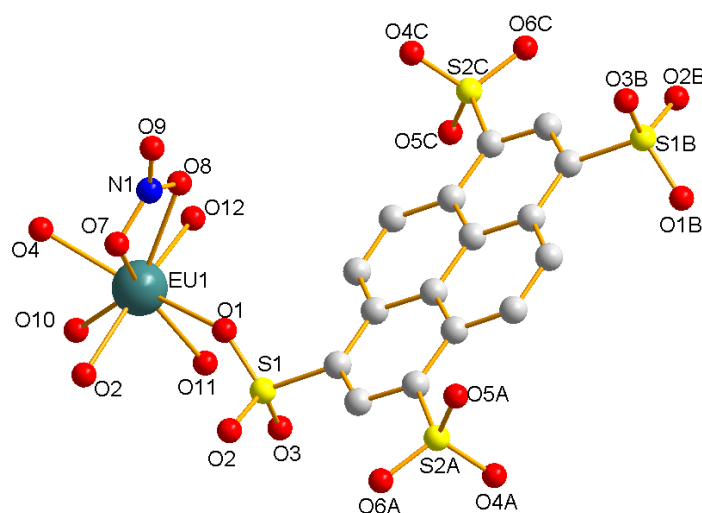


**Figure 4.** Coordination environment of the Eu(III) ions in compound **2**. Symmetry codes: (A)  $x, y, z - 1$ ; (B)  $-x + 1, -y + 1, -z$ ; (C)  $-x + 1, -y + 1, -z + 1$  (the H atoms were omitted for clarity).

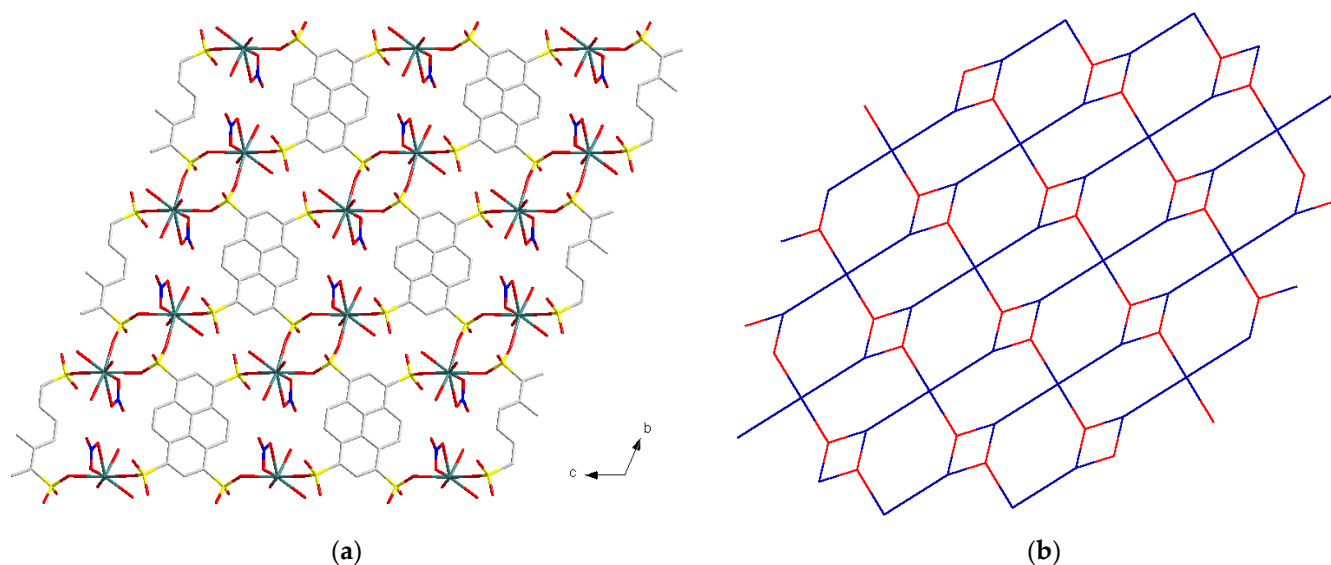


**Figure 5.** (a) Two-dimensional layered structure and (b) corresponding topological diagram in compound 2.

The spatial structure of compound 2 is formed by the stacking of pyrene tetra-sulfonic acid ligands in each layer through 4,4'-bipyridine molecules between layers, as shown in Figure 6. It can be speculated that 4,4'-bipyridine molecules play a template role in the synthesis of this compound.

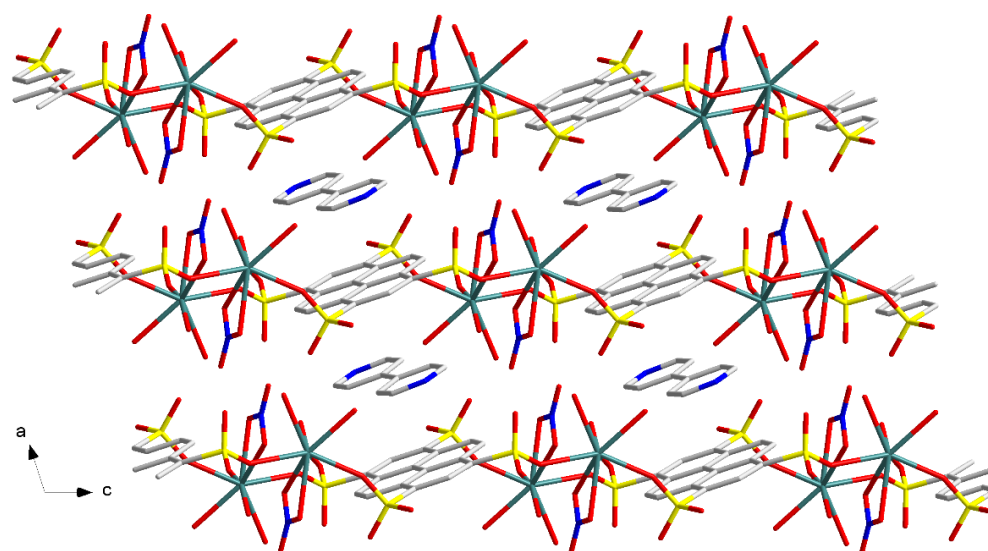


**Figure 6.** The packing structure in compound 2.

### 3.2. Structure Comparison and Formation Mechanism Speculation for EuPTS-CPs

As mentioned above, the compound **EuPTSbp-1** has a 1D snake-shaped structure in which the 4,4'-bipyridine auxiliary template acts as an important media of the  $\pi$ - $\pi$  stacking effect, eventually leading to the formation of such a structure. It is synthesized by the solvothermal method, where the molar ratio of metal/PTS ligand is 1:1 and the volume ratio of mixed  $\text{H}_2\text{O}$ /EtOH solvent is also 1:1.

To regulate the crystal structure of the product, the volume ratio of mixed  $\text{H}_2\text{O}$ /EtOH solvent was modulated to be 1:9 and the other reaction conditions including reactant ratio remain unchanged. The obtained compound **1** shows a 1D chains structure, which is similar to **EuPTSbp-1** (Figure 7). The coordination modes of the PTS ligands in these two compounds are the same too. In this way, only two para-sulfonic acid groups are

involved in coordination, who connects one Eu(III) ions in a  $\eta^1$  way, respectively (the second line in Figure 8). The main difference is the coordination environment of Eu(III) ions. As shown in Figure 8, for compound **EuPTSbp-1**, the Eu(III) ion is coordinated with nine oxygen atoms, two of which belong to sulfonic acid groups of PTS ligands and the other seven oxygen atoms come from coordinated  $\text{H}_2\text{O}$  molecule. While the situation is different in compound **1**, presumptively owing to the reduction of  $\text{H}_2\text{O}$  content in mixed solvents, nitrate ionization becomes difficult in ethanol-rich solvents, leading to partially maintain chelated to Eu(III) ions and occupying two coordination sites. On the other hand, because of the strong coordination effect of hydroxide on rare earth ions [44,45], hydroxide and even  $\text{O}^{2-}$  ions ionized from  $\text{H}_2\text{O}$  molecules bridges with multiple Eu(III) ions in an efficient  $\mu_3$  even  $\mu_6$  bridging mode result to form an hexanuclear europium oxygen cluster nod, so that the relatively scarce hydroxides in ethanol-rich solvents can be fully utilized. As a rough estimate, each Eu(III) ion coordinates with seven  $\text{H}_2\text{O}$  molecules in **EuPTSbp-1**, while six Eu(III) ions only share fifteen hydroxide or  $\text{O}^{2-}$  ions ionized from  $\text{H}_2\text{O}$ .

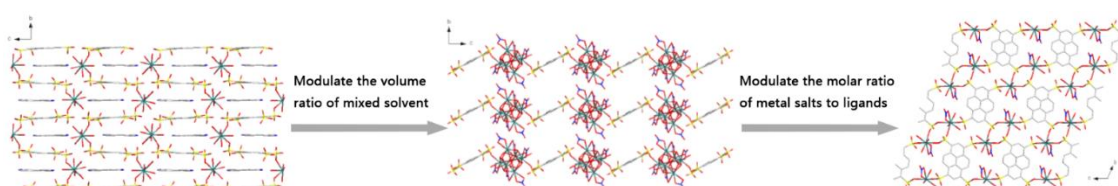


**Figure 7.** The structure regulation schematic diagram from **EuPTSbp-1** through **1** to **2**.

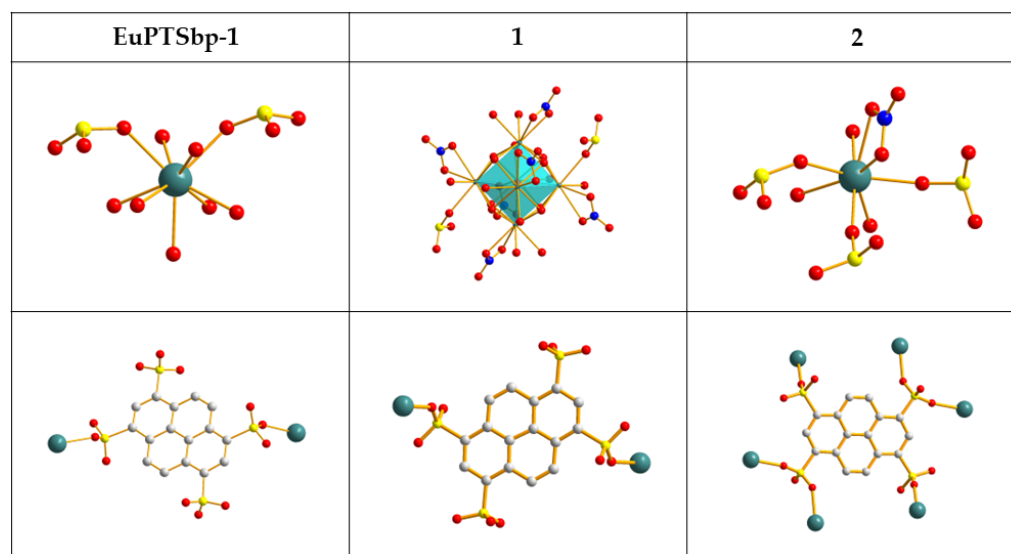


**Figure 8.** The coordination modes of Eu(III) ions and of pyrene tetra-sulfonic acid ligands in three different Eu-PTS MOCPs. Jasper: Eu; Red: O; Yellow: S; Blue: N; Offwhite: C (hydrogen atoms are omitted for clarity).

It is worth mentioning that, except for the different ligands and other non-bridged coordination groups such as coordinated water molecules and nitrate ions, the hexanuclear  $[\text{Eu}_6(\mu_6\text{-O})(\mu_3\text{-OH})_8(\text{NO}_3)_6]^{2+}$  clusters in compound **1** are almost identical to the lanthanide-based octahedral hexanuclear complexes reported by Guillaume Calvez et al. [46], though different synthesis methods are used. The lanthanide-based octahedral hexanuclear complexes were synthesized by dropwise adding an aqueous solution of sodium hydroxide to a solution of lanthanide nitrate in a mixture water/ethanol (1:9) while vigorously magnetically stirring. Compared with the synthesis methods in this paper, it is not difficult to find that the reaction products are both obtained in an alkaline mixture water/ethanol solution environment (1:9) in these two different synthetic methods. This is not entirely

a coincidence. It is well known that the lanthanide ions are easily hydrolyzed in water-rich environments to form stable polymeric species such as  $\text{Ln}(\text{OH})_2\text{NO}_3$ ,  $\text{LnONO}_3$ , and  $\text{Ln}(\text{OH})_3$  [47–49]. Reacting in an alkaline mixture water/ethanol solution environment seems to be necessary to inhibit the hydration of lanthanide ions.

Furthermore, several derived complexes based on this previous reported lanthanide-based octahedral hexanuclear complexes have been reported [50–54]. In these studies, a sequential synthesis strategy was used by means of substituting coordination groups on the base of pre-synthesized lanthanide-based octahedral hexanuclear complexes, which indicates a new research direction for the optimization of synthesis methods for compound **1** and even for the development of a family of MOCPs constructed by the lanthanide-based octahedral hexanuclear complexes as net nodes.

Furtherly, based on the synthesis conditions of compound **1**, the molar ratio of metal/ligands was modulated to be 15:1.25 and the other reaction conditions remain the same. Here, the metal salts are severely excessive in comparison with ligands. The obtained compound **2** turns out to be a 2D layered structure, which is packed by the  $\pi$ – $\pi$  stacking effect with the help of the 4,4'-bipyridine auxiliary template (Figure 7). Obviously, high concentrations Eu(III) ions cause each PTS ligand coordinate to have six Eu(III) instead of two. It should be noted that all the four sulfonic acid groups of PTS ligand are involved in the coordination to Eu(III) ions, and the coordination modes include  $\eta^1$  and  $\eta^2$ - $\mu_2$ , which highlights the richness and flexibility of the coordination modes of sulfonic acid ligands. It is worth mentioning that the coordination modes of Eu(III) ions are unlike that of the compound **1**, which has a hexanuclear europium oxygen cluster, with neither similar than the compound **EuPTSbp-1**. As a synthetic product in the same solvent ratio with compound **1**, chelated nitrate ions still occupies two coordination sites in compound **2**, which is the same as the former. Because of the domination of sulfonic acid group coordination and the space steric hindrance effect of PTS ligands, only three coordination sites are left for  $\text{H}_2\text{O}$  molecules, which eventually leads to an eight-coordination mode of Eu(III) ion.

In summary, the coordination habit of rare earth ions and the coordination modes of sulfonic acid ligands are both diverse and flexible. Modulating the solvent environment could regulate the coordination modes of rare ions, and modulating the metal/ligands molar ratio could stimulate or inhibit the coordination of sulfonic acid groups of ligands. This allows sequential modulation on the coordination modes of rare-earth metal ions and aryl sulfonate acid ligands, presenting a new way for structure regulation of sulfonic acid coordination polymers.

**Supplementary Materials:** The following supporting information can be downloaded at <https://www.mdpi.com/article/10.3390/cryst12121818/s1>. Table S1: Nearest metal–metal distance and main bond length and bond angle in compound **1**; Table S2: Nearest metal–metal distance and main bond length and bond angle in compound **2**; Figure S1: ORTEP representation of the asymmetric unit of compound **1**; Figure S2: Topological diagram for compound **1**; Figure S3: ORTEP representation of the asymmetric unit of compound **2**.

**Author Contributions:** H.L. conceived the idea, carried out the experimentation, and supervised the project. H.L. and X.S. wrote the draft of the manuscript and revised the manuscript with comments from J.F. and W.Z. All authors have read and agreed to the published version of the manuscript.

**Funding:** W.Z. would like to acknowledge the support from the Fundamental Research Funds for the Central Universities (021114380183, 021114380189, 021114380199), the Research Funds from Frontiers Science Center for Critical Earth Material Cycling of Nanjing University, and Research Funds for Jiangsu Distinguished Professor. This work was also supported by the National Natural Science Foundation of China (82272138, 81971738); Jiangsu Province Outstanding Youth Fund (BK20220086); Double first class Fund, China Pharmaceutical University (CPUQNJ22\_03); the Project Program of Key Laboratory of Drug Quality Control and Pharmacovigilance, China Pharmaceutical University (DQCP20/21MS02); the Natural Science Foundation of the Jiangsu Higher Education Institutions of China (21KJB510005); and Research Foundation of NJUIT (YK20-12-01).

**Data Availability Statement:** Not applicable.

**Conflicts of Interest:** The authors declare no conflict of interest.

## References

1. Tu, M.; Xia, B.Z.; Kravchenko, D.E.; Tietze, M.L.; Cruz, A.J.; Stassen, I.; Hauffman, T.; Teyssandier, J.; De Feyter, S.; Wang, Z.; et al. Direct X-ray and electron-beam lithography of halogenated zeolitic imidazolate frameworks. *Nat. Mater.* **2021**, *20*, 93–99. [[CrossRef](#)] [[PubMed](#)]
2. Cheng, W.R.; Zhao, X.; Su, H.; Tang, F.M.; Che, W.; Zhang, H.; Liu, Q.H. Lattice-strained metal-organic-framework arrays for bifunctional oxygen electrocatalysis. *Nat. Energy* **2019**, *4*, 115–122. [[CrossRef](#)]
3. Arora, H.; Dong, R.H.; Venanzi, T.; Zscharschuch, J.; Schneider, H.; Helm, M.; Feng, X.L.; Canovas, E.; Erbe, A. Demonstration of a Broadband Photodetector Based on a Two-Dimensional Metal-Organic Framework. *Adv. Mater.* **2020**, *32*, 7. [[CrossRef](#)] [[PubMed](#)]
4. Dou, Y.; Yang, L.; Qin, L.; Dong, Y.H.; Zhou, Z.; Zhang, D.P.; Wang, S.N. Self-assembly of a cobalt(II)-based metal-organic framework as an effective water-splitting heterogeneous catalyst for light-driven hydrogen production. *Acta Crystallogr. Sect. C-Struct. Chem.* **2020**, *76*, 616–624. [[CrossRef](#)]
5. Chen, S.S.; Han, S.S.; Ma, C.B.; Li, W.D.; Zhao, Y. A Series of Metal-Organic Frameworks: Syntheses, Structures and Luminescent Detection, Gas Adsorption, Magnetic Properties. *Cryst. Growth Des.* **2021**, *21*, 869–885. [[CrossRef](#)]
6. Du, H.; Fu, J.; Liu, L.-X.; Ding, S.; Lyu, Z.; Chang, Y.-C.; Jin, X.; Kengara, F.O.; Song, B.; Min, Q.; et al. Recent progress in electrochemical reduction of carbon monoxide toward multi-carbon products. *Mater. Today* **2022**, *59*, 182–199. [[CrossRef](#)]
7. Lu, T.Q.; Cheng, L.T.; Wang, X.T.; Chen, C.; Zheng, J.; Lu, D.F.; Zheng, X.Y. Lanthanide Metal-Organic Frameworks with High Chemical Stability as Multifunctional Materials: Cryogenic Magnetic Cooler and Luminescent Probe. *Cryst. Growth Des.* **2022**, *22*, 4917–4925. [[CrossRef](#)]
8. Zheng, W.; Guo, H.; Zhu, C.; Yue, C.; Zhu, W.; Liu, F.; Chen, Z.-X. Ultralow-Energy-Barrier H<sub>2</sub>O<sub>2</sub> Dissociation on Coordinatively Unsaturated Metal Centers in Binary Ce-Fe Prussian Blue Analogue for Efficient and Stable Photo-Fenton Catalysis. *Energy Environ. Mater.* **2022**, e12476. [[CrossRef](#)]
9. Sun, Z.; Sun, J.; Xi, L.; Xie, J.; Wang, X.F.; Ma, Y.; Li, L.C. Two Novel Lanthanide Metal-Organic Frameworks: Selective Luminescent Sensing for Nitrobenzene, Cu<sup>2+</sup>, and MnO<sub>4</sub>. *Cryst. Growth Des.* **2020**, *20*, 5225–5234. [[CrossRef](#)]
10. Niu, X.; Li, X.; Lyu, Z.; Pan, J.; Ding, S.; Ruan, X.; Zhu, W.; Du, D.; Lin, Y. Metal-organic framework based nanozymes: Promising materials for biochemical analysis. *Chem. Commun.* **2020**, *56*, 11338–11353. [[CrossRef](#)]
11. Lu, B.-B.; Han, X.; Feng, C.-J.; Wang, D.; Ye, F. Two Co(II)-Based MOFs Constructed from Resorcin[4]Arene Ligand: Syntheses, Structures, and Heterogeneous Catalyst for Conversion of CO<sub>2</sub>. *Crystals* **2021**, *11*, 574. [[CrossRef](#)]
12. Mahmoud, E. Quantitative Structure–Property Relationships from Experiments for CH<sub>4</sub> Storage and Delivery by Metal–Organic Frameworks. *Crystals* **2020**, *10*, 700. [[CrossRef](#)]
13. Du, H.; Liu, L.-X.; Cai, Y.; Wang, Y.; Zhang, J.-R.; Min, Q.; Zhu, W. In situ formed N-containing copper nanoparticles: A high-performance catalyst toward carbon monoxide electroreduction to multicarbon products with high faradaic efficiency and current density. *Nanoscale* **2022**, *14*, 7262–7268. [[CrossRef](#)] [[PubMed](#)]
14. Abdolalian, P.; Morsali, A. Flexible and breathing metal-organic framework with high and selective carbon dioxide storage versus nitrogen. *Polyhedron* **2019**, *161*, 56–62. [[CrossRef](#)]
15. Mahmoud, E.; Ali, L.; El Sayah, A.; Alkhatib, S.A.; Abdulsalam, H.; Juma, M.; Al-Muhtaseb, A.a.H. Implementing Metal-Organic Frameworks for Natural Gas Storage. *Crystals* **2019**, *9*, 406. [[CrossRef](#)]
16. Cho, W.; Park, S.; Oh, M. Coordination polymer nanorods of Fe-MIL-88B and their utilization for selective preparation of hematite and magnetite nanorods. *Chem. Commun.* **2011**, *47*, 4138–4140. [[CrossRef](#)]
17. Kong, A.; Mao, C.; Lin, Q.; Wei, X.; Bu, X.; Feng, P. From cage-in-cage MOF to N-doped and Co-nanoparticle-embedded carbon for oxygen reduction reaction. *Dalton Trans.* **2015**, *44*, 6748–6754. [[CrossRef](#)]
18. Liu, B.; Shioyama, H.; Akita, T.; Xu, Q. Metal-Organic Framework as a Template for Porous Carbon Synthesis. *J. Am. Chem. Soc.* **2008**, *130*, 5390–5391. [[CrossRef](#)]
19. Zhu, W.; Shen, M.; Fan, G.; Yang, A.; Meyer, J.R.; Ou, Y.; Yin, B.; Fortner, J.; Foston, M.; Li, Z.; et al. Facet-Dependent Enhancement in the Activity of Bismuth Vanadate Microcrystals for the Photocatalytic Conversion of Methane to Methanol. *ACS Appl. Nano Mater.* **2018**, *1*, 6683–6691. [[CrossRef](#)]
20. He, Y.H.; Hwang, S.; Cullen, D.A.; Uddin, M.A.; Langhorst, L.; Li, B.Y.; Karakalos, S.; Kropf, A.J.; Wegener, E.C.; Sokolowski, J.; et al. Highly active atomically dispersed CoN<sub>4</sub> fuel cell cathode catalysts derived from surfactant-assisted MOFs: Carbon-shell confinement strategy. *Energy Environ. Sci.* **2019**, *12*, 250–260. [[CrossRef](#)]
21. Niu, X.; Shi, Q.; Zhu, W.; Liu, D.; Tian, H.; Fu, S.; Cheng, N.; Li, S.; Smith, J.N.; Du, D.; et al. Unprecedented peroxidase-mimicking activity of single-atom nanozyme with atomically dispersed Fe–Nx moieties hosted by MOF derived porous carbon. *Biosens. Bioelectron.* **2019**, *142*, 111495. [[CrossRef](#)] [[PubMed](#)]
22. Yang, S.J.; Nam, S.; Kim, T.; Im, J.H.; Jung, H.; Kang, J.H.; Wi, S.; Park, B.; Park, C.R. Preparation and Exceptional Lithium Anodic Performance of Porous Carbon-Coated ZnO Quantum Dots Derived from a Metal–Organic Framework. *J. Am. Chem. Soc.* **2013**, *135*, 7394–7397. [[CrossRef](#)] [[PubMed](#)]
23. Tang, J.; Salunkhe, R.R.; Liu, J.; Torad, N.L.; Imura, M.; Furukawa, S.; Yamauchi, Y. Thermal Conversion of Core–Shell Metal–Organic Frameworks: A New Method for Selectively Functionalized Nanoporous Hybrid Carbon. *J. Am. Chem. Soc.* **2015**, *137*, 1572–1580. [[CrossRef](#)] [[PubMed](#)]

24. Wang, G.; Li, X.; Yang, X.; Liu, L.-X.; Cai, Y.; Wu, Y.; Wang, S.; Li, H.; Zhou, Y.; Wang, Y.; et al. Metal-Based Aerogels Catalysts for Electrocatalytic CO<sub>2</sub> Reduction. *Chem. A Eur. J.* **2022**, *28*, e202201834. [[CrossRef](#)]
25. Liu, J.; Cai, Y.; Song, R.; Ding, S.; Lyu, Z.; Chang, Y.-C.; Tian, H.; Zhang, X.; Du, D.; Zhu, W.; et al. Recent progress on single-atom catalysts for CO<sub>2</sub> electroreduction. *Mater. Today* **2021**, *48*, 95–114. [[CrossRef](#)]
26. Xu, X.; Cao, R.; Jeong, S.; Cho, J. Spindle-like Mesoporous  $\alpha$ -Fe<sub>2</sub>O<sub>3</sub> Anode Material Prepared from MOF Template for High-Rate Lithium Batteries. *Nano Lett.* **2012**, *12*, 4988–4991. [[CrossRef](#)] [[PubMed](#)]
27. Zhou, H.-F.; He, T.; Yue, K.-F.; Liu, Y.-L.; Zhou, C.-S.; Yan, N.; Wang, Y.-Y. Temperature-Induced Syntheses, Iodine Elimination, Enantiomers Resolution, and Single-Crystal-to-Single-Crystal Transformation of Imidazole-Co(II) Coordination Polymers with Amino-isophthalic Acid as Co-Ligand. *Cryst. Growth Des.* **2016**, *16*, 3961–3968. [[CrossRef](#)]
28. Wang, Z.; Hu, K.; Gao, S.; Kobayashi, H. Formate-Based Magnetic Metal–Organic Frameworks Templated by Protonated Amines. *Adv. Mater.* **2010**, *22*, 1526–1533. [[CrossRef](#)]
29. Mazaj, M.; Birsa Čelič, T.; Mali, G.; Rangus, M.; Kaučič, V.; Zabukovec Logar, N. Control of the Crystallization Process and Structure Dimensionality of Mg–Benzene–1,3,5-Tricarboxylates by Tuning Solvent Composition. *Cryst. Growth Des.* **2013**, *13*, 3825–3834. [[CrossRef](#)]
30. Feng, Y.; Wang, D.-B.; Wan, B.; Li, X.-H.; Shi, Q. Construction of 1D to 3D cadmium(II) coordination polymers from 4-(imidazol-1-yl)-benzoic acid: Effect of bridging anions. *Inorg. Chim. Acta* **2014**, *413*, 187–193. [[CrossRef](#)]
31. Liu, K.; Hu, H.; Sun, J.; Zhang, Y.; Han, J.; Wang, L. pH-value-controlled assembly of photoluminescent zinc coordination polymers in the mixed-ligand system. *J. Mol. Struct.* **2017**, *1134*, 174–179. [[CrossRef](#)]
32. Shimizu, G.K.; Enright, G.D.; Ratcliffe, C.I.; Preston, K.F.; Reid, J.L.; Ripmeester, J.A. A layered silver sulfonate incorporating nine-coordinate AgI in a hexagonal grid. *Chem. Commun.* **1999**, *16*, 1485–1486. [[CrossRef](#)]
33. Cai, J. Structural chemistry and properties of metal arenesulfonates. *Coord. Chem. Rev.* **2004**, *248*, 1061–1083. [[CrossRef](#)]
34. Côté, A.P.; Shimizu, G.K.H. The supramolecular chemistry of the sulfonate group in extended solids. *Coord. Chem. Rev.* **2003**, *245*, 49–64. [[CrossRef](#)]
35. Meng, X.; Song, S.-Y.; Song, X.-Z.; Zhu, M.; Zhao, S.-N.; Wu, L.-L.; Zhang, H.-J. A tetranuclear copper cluster-based MOF with sulfonate–carboxylate ligands exhibiting high proton conduction properties. *Chem. Commun.* **2015**, *51*, 8150–8152. [[CrossRef](#)] [[PubMed](#)]
36. Zhang, G.; Wei, G.; Liu, Z.; Oliver, S.R.J.; Fei, H. A Robust Sulfonate-Based Metal–Organic Framework with Permanent Porosity for Efficient CO<sub>2</sub> Capture and Conversion. *Chem. Mater.* **2016**, *28*, 6276–6281. [[CrossRef](#)]
37. D’Vries, R.F.; de la Peña-O’Shea, V.A.; Snejko, N.; Iglesias, M.; Gutiérrez-Puebla, E.; Monge, M.Á. Insight into the Correlation between Net Topology and Ligand Coordination Mode in New Lanthanide MOFs Heterogeneous Catalysts: A Theoretical and Experimental Approach. *Cryst. Growth Des.* **2012**, *12*, 5535–5545. [[CrossRef](#)]
38. Li, H.; Sheng, T.; Xue, Z.; Zhu, X.; Hu, S.; Wen, Y.; Fu, R.; Zhuo, C.; Wu, X. Synthesis, structure, characterization, and multifunctional properties of a family of rare earth organic frameworks. *Crystengcomm* **2017**, *19*, 2106–2112. [[CrossRef](#)]
39. Demel, J.; Kubát, P.; Millange, F.; Marrot, J.; Císařová, I.; Lang, K. Lanthanide-Porphyrin Hybrids: From Layered Structures to Metal–Organic Frameworks with Photophysical Properties. *Inorg. Chem.* **2013**, *52*, 2779–2786. [[CrossRef](#)]
40. Zhu, W.; Yu, H.; Zhu, X.; Li, H. A luminescence europium Metal-organic coordination polymer for Room-Temperature X-ray detection. *Inorg. Chem. Commun.* **2022**, *136*, 109182. [[CrossRef](#)]
41. Dolomanov, O.V.; Bourhis, L.J.; Gildea, R.J.; Howard, J.A.K.; Puschmann, H. OLEX2: A complete structure solution, refinement and analysis program. *J. Appl. Crystallogr.* **2009**, *42*, 339–341. [[CrossRef](#)]
42. Bourhis, L.J.; Dolomanov, O.V.; Gildea, R.J.; Howard, J.A.K.; Puschmann, H. The anatomy of a comprehensive constrained, restrained refinement program for the modern computing environment—Olex2 dissected. *Acta Crystallogr. Sect. A* **2015**, *71*, 59–75. [[CrossRef](#)] [[PubMed](#)]
43. Sheldrick, G. SHELXT—Integrated space-group and crystal-structure determination. *Acta Crystallogr. Sect. A* **2015**, *71*, 3–8. [[CrossRef](#)] [[PubMed](#)]
44. Gu, X.; Xue, D. Selected Controlled Synthesis of Three-Dimensional 4d–4f Heterometallic Coordination Frameworks by Lanthanide Carboxylate Subunits and Silver Centers. *Cryst. Growth Des.* **2006**, *6*, 2551–2557. [[CrossRef](#)]
45. Yan, C.; Li, K.; Wei, S.-C.; Wang, H.-P.; Fu, L.; Pan, M.; Su, C.-Y. Lanthanide homometallic and d–f heterometallic MOFs from the same tripodal ligand: Structural comparison, one photon (OP) vs. two photon (TP) luminescence and selective guest adsorption behavior. *J. Mater. Chem.* **2012**, *22*, 9846–9852. [[CrossRef](#)]
46. Calvez, G.; Daiguebonne, C.; Guillou, O.; Le Dret, F. A New Series of Anhydrous Lanthanide-Based Octahedral Hexanuclear Complexes. *Eur. J. Inorg. Chem.* **2009**, *2009*, 3172–3178. [[CrossRef](#)]
47. Müller, A.; Krickemeyer, E.; Bögge, H.; Schmidtman, M.; Peters, F. Organizational Forms of Matter: An Inorganic Super Fullerene and Keplerate Based on Molybdenum Oxide. *Angew. Chem. Int. Ed.* **1998**, *37*, 3359–3363. [[CrossRef](#)]
48. Beall, G.W.; Milligan, W.O.; Dillin, D.R.; Williams, R.J.; McCoy, J.J. Refinement of neodymium trihydroxide. *Acta Crystallogr. Sect. B* **1976**, *32*, 2227–2229. [[CrossRef](#)]
49. Pelloquin, D.; Louër, M.; Louër, D. Powder Diffraction Studies in the YONO<sub>3</sub>–Y<sub>2</sub>O<sub>3</sub> System. *J. Solid State Chem.* **1994**, *112*, 182–188. [[CrossRef](#)]

50. Le Natur, F.; Calvez, G.; Daiguebonne, C.; Guillou, O.; Bernot, K.; Ledoux, J.; Le Polles, L.; Roiland, C. Coordination polymers based on heterohexanuclear rare earth complexes: Toward independent luminescence brightness and color tuning. *Inorg. Chem.* **2013**, *52*, 6720–6730. [[CrossRef](#)]
51. Yao, H.; Calvez, G.; Daiguebonne, C.; Bernot, K.; Suffren, Y.; Guillou, O. Hetero-hexalanthanide Complexes: A New Synthetic Strategy for Molecular Thermometric Probes. *Inorg. Chem.* **2019**, *58*, 16180–16193. [[CrossRef](#)] [[PubMed](#)]
52. Yao, H.; Calvez, G.; Daiguebonne, C.; Bernot, K.; Suffren, Y.; Puget, M.; Lescop, C.; Guillou, O. Hexalanthanide Complexes as Molecular Precursors: Synthesis, Crystal Structure, and Luminescent and Magnetic Properties. *Inorg. Chem.* **2017**, *56*, 14632–14642. [[CrossRef](#)]
53. Yao, H.; Calvez, G.; Daiguebonne, C.; Suffren, Y.; Bernot, K.; Guillou, O. Hexanuclear Molecular Precursors as Tools to Design Luminescent Coordination Polymers with Lanthanide Segregation. *Inorg. Chem.* **2021**, *60*, 16782–16793. [[CrossRef](#)] [[PubMed](#)]
54. Yao, H.; Calvez, G.; Daiguebonne, C.; Suffren, Y.; Bernot, K.; Guillou, O. Microwave-assisted synthesis of lanthanide coordination polymers with 2-bromobenzoic acid as ligand from hexa-lanthanide molecular precursors. *J. Mol. Struct.* **2022**, *1250*, 131918. [[CrossRef](#)]